Biomedicine & Pharmacotherapy 151 (2022) 113172

Contents lists available at ScienceDirect

Biomedicine & Pharmacotherapy

journal homepage: www.elsevier.com/locate/biopha

Endothelium-targeted delivery of PPARδ by adeno-associated virus serotype 1 ameliorates vascular injury induced by hindlimb ischemia in obese mice

Yalan Wu [a,b,c,1], Xiao Lin [d,1], Huiling Hong [a,b,c], Yee Lok Fung [a,b,c], Xiaoyun Cao [a,b,c], Joyce Ka Yu Tse [d], Tsz Ho Li [d], Ting Fung Chan [c,d], Xiao Yu Tian [a,b,c,*]

[a] Chinese University of Hong Kong, Hong Kong, China
[b] School of Biomedical Sciences, Faculty of Medicine, Hong Kong, China
[c] Shenzhen Research Institute, Chinese University of Hong Kong, Shenzhen, China
[d] School of Life Sciences, Chinese University of Hong Kong, Hong Kong, China

ARTICLE INFO

Keywords:
PPARδ
AAV1
Gene therapy
Hindlimb ischemia

ABSTRACT

Diabetic vasculopathy is a major health problem worldwide. Peripheral arterial disease (PAD), and in its severe form, critical limb ischemia is a major form of diabetic vasculopathy with limited treatment options. Existing literature suggested an important role of PPARδ in vascular homeostasis. It remains elusive for using PPARδ as a potential therapeutic target due to mostly the side effects of PPARδ agonists. To explore the roles of PPARδ in endothelial homeostasis, endothelial cell (EC) selective *Ppard* knockout and controlled mice were subjected to hindlimb ischemia (HLI) injury. The muscle ECs were sorted for single-cell RNA sequencing (scRNA-seq) analysis. HLI was also performed in high fat diet (HFD)-induced obese mice to examine the function of PPARδ in obese mice with delayed vascular repair. Adeno-associated virus type 1 (AAV1) carrying ICAM2 promoter to target endothelium for overexpressing PPARδ was injected into the injured muscles of normal chow- and HFD-fed obese mice before HLI surgery was performed. scRNA-seq analysis of ECs in ischemic muscles revealed a pivotal role of PPARδ in endothelial homeostasis. PPARδ expression was diminished both after HLI injury, and also in obese mice, which showed further delayed vascular repair. Endothelium-targeted delivery of PPARδ by AAV1 improved perfusion recovery, increased capillary density, restored endothelial integrity, suppressed vascular inflammation, and promoted muscle regeneration in ischemic hindlimbs of both lean and obese mice. Our study indicated the effectiveness of endothelium-targeted PPARδ overexpression for restoring functional vasculature after ischemic injury, which might be a promising option of gene therapy to treat PAD and CLI.

1. Introduction

Diabetic vasculopathy is the major cause of morbidity and mortality in the diabetic population [1]. Diabetic patients have a higher risk of developing atherosclerosis, which is the most common cause of peripheral arterial disease (PAD) [2]. Peripheral arterial disease (PAD) is an atherosclerotic cardiovascular disease characterized by narrowing and occlusion of the arteries that supply blood and nutrient to the lower extremities, which affects over 236 million people worldwide [3], with higher incidence approximately at 20% of the population aged 60 or older [4]. PAD, if untreated, could develop into more severe disease as critical limb ischemia (CLI). Currently, anti-inflammation, stimulating revascularization and muscle regeneration are the key avenues for treating CLI. However, due to lack of effective therapeutic targets and avenues to achieve multi-advantages, CLI patients are risky to suffer much worse outcomes among all atherosclerotic ischemic diseases than the other more common manifestation of atherosclerotic disease including coronary artery disease (CAD) and cerebrovascular disease.

Obesity is strongly associated with insulin resistance [5] and atherosclerosis [6]. In general population, obesity and insulin resistance

* Correspondence to: Lo-Kwee Seong Integrated Biomedical Sciences Building School of Biomedical Sciences Chinese University of Hong Kong, Room 208, Shatin, NT, Hong Kong, China.
E-mail address: xytian@cuhk.edu.hk (X.Y. Tian).
[1] Co-first author.

https://doi.org/10.1016/j.biopha.2022.113172
Received 15 April 2022; Received in revised form 13 May 2022; Accepted 22 May 2022
Available online 26 May 2022

are positively associated with the incidence of hospitalized PAD, independent of potential confounders, especially its most severe form of CLI [7]. A study indicated that substantially greater inflammatory, pro-thrombotic, and genomic stress responses in diet-induced obese mice after hindlimb ischemia compared to normal diet mice [8]. However, options of clinical prevention and therapy with promising targets and methods are still limited.

Over the past two decades, there have been many viral vector-based gene therapy methods tested for severe inherited diseases, for example primary immunodeficiencies, leukodystrophies, thalassaemia, haemophilia and retinal dystrophy [9]. These diseases even entered into phase I/II gene-therapy clinical trials and exhibited good efficacy and safety, indicating that gene therapy is clinically effective and well tolerated for rare genetic disorders and, perhaps for other chronic diseases as well. Gene therapy to promote therapeutic neovascularization is a promising approach for the treatment of myocardial and peripheral ischemia [10]. In addition, selection of a proper delivering agent and a reasonable target gene also affects the effectiveness of this procedure.

Recombinant adeno-associated viral vector type 1 (rAAV1), which exhibits more efficient and faster transgene expression than rAAV2 in skeletal muscle [11,12] has also been used in clinical trials including the treatment of antitrypsin deficiency [13] lipoprotein lipase deficiency [14], Pompe disease (ClinicalTrials.gov number NCT00976352), and muscular dystrophy [15]. Notably, an rAAV1 vector encoding the lipoprotein lipase was approved in 2012 for the treatment of patients with this enzyme deficiency [16]. This marks the first realization of gene therapy as a feasible clinical treatment strategy. Despite the above-mentioned success, there are still several obstacles in the clinical applications of AAV vector systems for gene therapy. For example, the pre-existing immunity due to antibody-mediated neutralization after natural AAV infections, which is common in humans, could limit the efficacy of AAV gene transduction in animal models and human clinical trials, even when the in vivo pre-existing anti-AAV antibodies titers are at relatively low levels [17,18]. For this reason, hemophilia B of clinical trial using the rAAV8 vector excludes individuals who had pre-existing AAV antibodies [19].

Cell-selective expression can be achieved by the use of tissue-specific promoters that drive gene expression using AAV. This method provides advantages for targeting organ-specific diseases, while avoiding potential undesirable effects in other health tissues or organs. Taking cardiovascular diseases for example, a previous study showed that AAV9-overexpressing PFKFB3 in muscle myotubes and endothelial cells protects muscles from ischemic injury by enhancing glycolytic metabolism [20]. Another study showed that delivering several genes including Gata4, Mef2c, Tbx5, and Tβ4 (thymosin β4) by AAV to target cardiac fibroblasts facilitated reprogramming and regeneration in mouse model of myocardial infarction [21].

Peroxisome proliferator-activated receptor δ (PPARδ) has long been known as a member of nuclear receptor superfamily of ligand-activated transcription factors [22]. The role of PPARδ in vascular biology have been quite well studied based on mostly ligand-induced activation and its downstream target genes and their effects. For instance, activation of PPARδ by agonist has profound benefits on vascular homeostasis and coronary artery disease [23,24]. However, some studies find that PPARδ agonists have unexpected side effects, for examples, promoting both angiogenesis and cancer progression [25–27], which largely limits its further application. Interestingly, our previous study demonstrates the protective effect of PPARδ on vascular homeostasis in a ligand-independent manner [28], which encourages us to explore the therapeutic efficacy basing on AAV-mediated delivery of PPARδ in endothelium.

In the present study, we aimed at investigating the endothelial selective roles of PPARδ in both normal- and high fat diet-induced obesity mice in hindlimb ischemia model, by applying rAAV1 serotype which carries an endothelium-selective promoter to drive PPARδ preferentially expressed in endothelial cells of skeletal muscle, to examine whether the outcomes of muscle ischemia are improved and whether the post-ischemic vascular repair is enhanced.

2. Materials and Methods

2.1. Animal studies

All animal experiments were approved by and were performed in the designated facilities accredited by the Animal Experimental Ethics Committee of the Chinese University of Hong Kong (approval number: 19–058-HMF and 20–073-GRF), and all the animal procedures were performed in the designated facilities accredited by the Animal Experimental Ethics Committee.

All the mice were maintained at 22 °C in a barrier facility and kept on a 12 h-light/12 h-dark cycle with free access to food and water. The *Ppard* floxed mutant mice (B6.129S4-*Ppard*^{tm1Rev}/J) (RRID: IMSR_JAX:005897) and the VEC-cre transgenic mice (B6;129-Tg*(Cdh5-cre)*^{1Spe}/J) (RRID:IMSR_JAX:017968) were originally obtained from Jackson laboratory. Both strains were backcrossed with C57BL/6 mice. *Ppard*$^{f/f}$ (*Ppard*$^{EC\text{-}WT}$) mice were crossed to VEC-Cre mice to generate endothelial cells selective deletion of *Ppard* as *Ppard*$^{f/f}$;*Cdh5*$^{Cre/+}$ (*Ppard*$^{EC\text{-}KO}$) mice [28].

For HFD treatment, eight-week-old male *Ppard*$^{EC\text{-}WT}$ and *Ppard*$^{EC\text{-}KO}$ mice were randomly grouped and fed either NC or a 60 kcal% HFD (D12492; Research Diets Inc., NJ, USA) for 12 weeks [29,30]. Body weight and blood glucose were measured after mice fed with 12-week HFD.

2.2. Hindlimb ischemia model and assessments

For single cell analysis and AAV injection in NC mice, ligation of common iliac artery to induce HLI was performed in 10-weeks old male mice [31,32]. For NC and HFD cohorts, ligation was performed at 12 weeks after HFD feeding. Mice were anesthetized via intraperitoneal injection of a combination of 75 mg/kg ketamine and 10 mg/kg xylazine (Alfasan Co, Netherlands). The iliac artery was exposed and ligated with two surgical knots. In this unilateral ischemia model, the contralateral limb was considered as control. Mice was kept warm on a heatpad at 36 ± 1.0 °C during the procedure and recovery.

For laser Doppler flow imaging analysis, all mice were anesthetized and maintained under 2% isoflurane in oxygen at the flow rate of 1 liter/min. Blood perfusion was measured by imaging of plantar regions with the Laser Speckle Contrast Imaging System RFLSI III (RWD Life Science Co.) and the average lower leg blood flow was presented as the ratio of ischemic to non-ischemic side at days 0, 3, 7, 14, 21 and 28 following HLI. Vasculature imaging of the thigh was performed with the Laser Speckle Contrast Imaging System RFLSI III (RWD Life Science Co., Shenzhen, Guangdong, China).

2.3. Histological analysis of skeletal muscle

GA muscle was harvested and embedded in OCT and frozen in 2-methylbutane cooled with liquid nitrogen. For H&E staining, 10 μm sections were fixed with 4% paraformaldehyde, and stained with hematoxylin and eosin with standard procedures. For Masson's trichrome staining, 10 μm sections were fixed in Mordant in Bouin's solution for 30 min, stained sequentially with Weigert's iron hematoxylin, Biebrich scarlet-acid fuchsin, phosphotungstic/phosphomolybdic acid, and aniline blue. All the sections were dehydrated and mounted with a xylene-based mounting medium.

2.4. Single cell isolation for flow cytometric analysis and scRNA-seq

GA muscles were harvested from injured leg of mice on 7 days after HLI surgery and digested with 800 U/ml Collagenase IV + 1 U/ml Neutral Protease (both from Worthington Biochemical, USA) for 1 h. To

generate single-cell suspensions, cells were suspended in FACS buffer (2% FBS with 2 mmol/L EDTA in PBS) after centrifuge and filtered through 40-μm cell strainer (BD Biosciences, USA). Cells were then incubated with LIVE/DEAD Aqua (Invitrogen, USA) for viability according to manufacturer's protocol together with anti-CD16/CD32 (1 μg/ml, Biolegend, USA) for 0.5 h on ice. Next, cells were incubated on ice with fluorescent-conjugated anti-mouse antibodies listed in Supplementary Table 1. Finally, cells were fixed with 1.6% paraformaldehyde for 0.5 h 4 ℃ until further analysis on FACSAria Fusion (BD Biosciences, USA). Data were analyzed using FlowJo. For scRNA-seq analysis, after incubated with LIVE/DEAD Aqua, cells were washed and stained with anti-CD45, anti-CD31, anti-CD144. $CD45^{-}CD31^{+}CD144^{+}$ labeled endothelial cells were sorted from FACSAria Fusion (BD Biosciences, USA) and resuspended in 0.4% BSA containing PBS after washed twice. Single cell RNA-seq libraries were prepared using the Chromium Single Cell 3′ Reagent Kits (v2 Chemistry) with the Chromium Controller (10x Genomics) as per the manufacturer's protocol. The libraries were sequenced on an Illumina NovoSeq 6000 (Novogene, Beijing, China).

2.5. Data processing and functional analysis for scRNA-seq

The raw sequencing data of individual samples, including $Ppard^{EC\text{-}WT}$ and $Ppard^{EC\text{-}KO}$, were processed using Cell Ranger (3.1.0) with the mouse reference genome and annotation (refdata-cellranger-mm10–3.0.0) (10x Genomics). Then, Seurat (3.1.5) [33] was used to perform downstream analyses based on the filtered feature barcode matrices generated by Cell Ranger (Fig. S1a). Briefly, cells of less than 200 or more than 6000 genes, as well as more than 5% mitochondrial reads, were filtered out. Normalization and variable features identification of individual samples were performed prior to integrating the two samples. For integrating the two samples, the first 30 dimensions of the canonical correlation vectors were used for anchoring. After integration, the cell cycle scores, including S phase and G2/M phase, which were calculated based on a previously reported list of cell cycle markers [34], the total RNA count and the percentage of expressed mitochondrial genes was used for data scaling. Principal component analysis was performed with the scaled expression data. The first 25 principal components were used for further dimension reduction using UMAP, as well as for cell clustering. The marker genes were identified based on the cell clustering result, with both "min.pct" and "logfc.threshold" set at 0.5 using the "FindAllMarkers" function, and differential expression analysis was performed between the two samples for each cluster, with "min.pct" set at 0.5 using the "FindMarkers" function. With the list of differentially expressed genes, the Ingenuity Pathway Analysis (IPA) software (Qiagen), was used for canonical pathway enrichment analysis for each cluster. In addition, the fold-changes of all genes between the two samples for each cluster were calculated, with both "min.pct" and "logfc.threshold" set at 0 using the "FindMarkers" function. These fold-change values were then ranked by the fold-change and used for gene set enrichment analysis [35] using the Molecular Signature Database hallmark gene set collection [36]. For the EC1 cluster, the marker genes were used for regulatory network analysis using IPA. The raw data could be assessed on NCBI with the accession ID: PRJNA691127.

2.6. Immunofluorescence staining

Frozen sections of GA muscle were fixed in cold acetone, blocked with normal goat or donkey serum (Abcam), and incubated with anti-CD144, anti-PPARδ, anti-CD63, anti-CD81, anti-VCAM1, anti-α-SMA, anti-VEGFR2, anti-Cldn5, anti-VEGFR1, anti-ZO-1 and appropriate fluorescence-conjugated secondary antibodies, followed by Hoechst 33342 (ThermoFisher) for nucleus, and mounted in fluorescence mounting medium (Electron Microscopy, Cat#17985–10). Detailed information of all the antibodies used can be found in Supplementary table 2.

2.7. Adeno-associated viruses (AAV) administration

For AAV1-mediated ICAM2-driven *Ppard* overexpression, ICAM2 promoter was synthesized and inserted into pAAV1 vector to replace the original CMV promoter. The ICAM2 core promoter sequence was previously reported [37], as follows: CCAAGGGCTGCCTGGAGGGA-GATGGTGGGCGCAGGTCTGAGCTATGGCCCA-GAATCCCTAGCCTTCTGCAAACTGATGACTGCATTTCCTCTCATTATCT-GAGAGATCTTTGGGAAGCCACGTGCACCAGCTCGTTCTAG. Then, the mouse *Ppard* CDS with fusion of Flag-tag was ligated into recombinant pAAV1-ICAM2 vector. All elements were verified by DNA sequencing. The production of AAV1-control and AAV1-*Ppard* was generated by Vigene Bioscience (WZ Biosciences Inc., Jinan, Shandong, China).

The viruses (total 10^{11} vg in 30 μL) were injected into GA, TA and quadriceps of both sides of the $Ppard^{EC\text{-}WT}$, $Ppard^{EC\text{-}KO}$ male mice 1 week before HLI was performed.

2.8. RNA extraction and qPCR

Total RNA was extracted from mouse GA or TA with TRIzol reagent RNAiso Plus (Takara, cat# 9109) and 1 μg of total RNA was reversely transcribed into complementary DNA (cDNA) using 5 × PrimeScript RT Master Mix (Takara, cat# RR036A) according to the manufacturer's instructions. The mRNA levels were determined by quantitative PCR with TB Green® Premix Ex Taq™ (Tli RNase H Plus (Takara, cat# RR420A) detected on an Applied Biosystems ViiA7. All primer sequences are listed in Supplementary table 2.

2.9. Statistical analysis

All data were presented as means ± SEM and the numbers of independent experiments are indicated. Student's t test was used for comparison between two samples, and one-way ANOVA and multiple comparison test was used for more than two samples in GraphPad Prism. * $p < 0.05$, * * $p < 0.01$, and * ** $p < 0.001$ were indicated as statistically significant.

3. Results

3.1. Single-cell profiling and unbiased clustering of endothelial cells from GA muscle of $Ppard^{EC\text{-}WT}$ and $Ppard^{EC\text{-}KO}$ mice after hindlimb ischemia

PPARδ is highly expressed in vascular tissue, especially the endothelium [38]. Although its roles in endothelial cells (ECs) are widely reported and relevant mechanisms are elucidated, whether PPARδ is a promising target for peripheral artery disease (PAD) is still needed more clarifications. Thus, we generated the endothelial selective Ppard knockout ($Ppard^{EC\text{-}KO}$) and wild type ($Ppard^{EC\text{-}WT}$) mice, to explore the effect of endothelial PPARδ deletion on endothelial function in the disease model of hindlimb ischemia (HLI). Firstly, we applied scRNA-seq to perform transcriptome profiling of $CD45^{-}CD31^{+}CD144^{+}$ ECs from the gastrocnemius (GA) muscles of $Ppard^{EC\text{-}KO}$ and $Ppard^{EC\text{-}WT}$ mice post hindlimb ischemia at days 7. ECs were FACS-sorted and filtered for scRNA-seq (Fig. 1a, b), following 10x Genomics-based single-tube protocol.

We used the Seurat package for scRNA-seq data filtering and processing (see Materials and Methods), i.e., excluding cells with less than 200 or more than 6000 genes, as well as more than 5% mitochondrial reads (Fig. S1a). As a result, the two samples were integrated into a unified transcriptomic atlas containing 10,148 cells, expressing a total of 17,278 detectable genes including estimated 6563 cell from $Ppard^{EC\text{-}WT}$ mice and 3585 cells from $Ppard^{EC\text{-}KO}$ mice, respectively (Fig. S1a).

Next, to annotate the cell types presenting in this ischemic muscle atlas, we employed uniform manifold approximation and projection (UMAP) to visualize the individual transcriptomes of all cells in the unified dataset (Fig. S1b). Finally, after optimizing the unsupervised

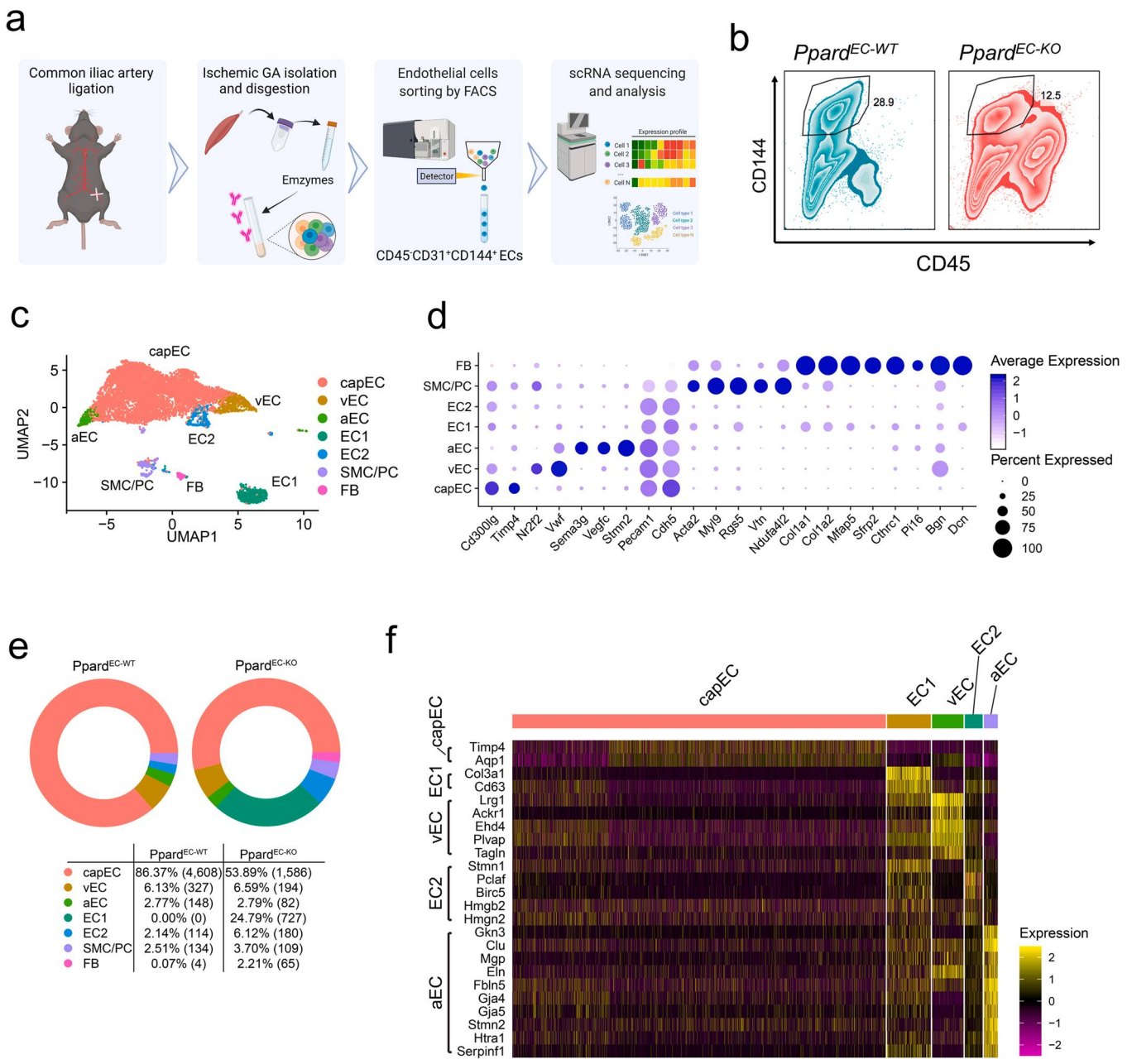

	Pparδ^EC-WT	Pparδ^EC-KO
capEC	86.37% (4,608)	53.89% (1,586)
vEC	6.13% (327)	6.59% (194)
aEC	2.77% (148)	2.79% (82)
EC1	0.00% (0)	24.79% (727)
EC2	2.14% (114)	6.12% (180)
SMC/PC	2.51% (134)	3.70% (109)
FB	0.07% (4)	2.21% (65)

Fig. 1. Single-cell RNA sequencing analysis of endothelial cells derived from injured muscles of *Pparδ*$^{EC\text{-}WT}$and *Pparδ*$^{EC\text{-}KO}$ mice. (a) Schematic experimental procedure showing the single-cell RNA sequencing (scRNA-Seq) analysis of EC transcriptome. (b) Representative flow plots showing selected ECs from *Pparδ*$^{EC\text{-}WT}$ and *Pparδ*$^{EC\text{-}KO}$ mice for scRNA-Seq. (c) UMAP visualization of primary cell clusters based on marker gene expression patterns. Cell type abbreviations: capEC, capillary EC; vEC, venous EC; aEC, arterial EC; SMC, smooth muscle cell; PC, pericyte. (d) Dot plot displaying the core genes which identify EC clusters and the non-ECs. Dot size: proportion of cells within the group expressing indicated transcript. Dot color: expression level. (e) Pie chart showing the proportion of each cluster in respective genotype, and the table (lower) showing proportion and cell number for each cluster. (f) Heatmap presenting the enriched gene expression for each EC subtype from the analysis of combined scRNA-Seq data of both *Pparδ*$^{EC\text{-}WT}$ and *Pparδ*$^{EC\text{-}KO}$.

shared nearest neighbor (SNN) resolution parameter by silhouette analysis, total cells were clustered into 7 groups based on their transcriptomic programs (Fig. 1c). Further, to identify these populations, we examined the normalized expression level and frequency of canonical cell type genes and named them based on their exclusivity in these expression patterns, accordingly uncovering 5 EC clusters: aECs, capECs, vECs, EC1 and EC2 (Fig. 1c, d). In details, arterial ECs (aECs) highly expressed semaphoring 3 G (*Sema3g*) [39], and stathmin 2 (*Stmn2*) [40]; venule ECs (vECs) highly expressed *Nr2f2* [41,42] and *Vwf* [43]; whereas capillary ECs (capECs) highly expressed L-selectin ligand nepmucin (*Cd300lg*) [44], and *Timp4* [45]; as indicated in Fig. 1d. Notably, EC1 and EC2 cluster displayed distinct cluster specific expression profile and could not be classified using canonical markers. Nevertheless, all identified five EC clusters highly express both *Cdh5* (CD144) and *Pecam1* (CD31), which are well-defined EC markers (Fig. S1c, S1d). We also identified SMC/PC (smooth muscle cells and pericytes) and FB (fibroblasts) clusters which might be contaminated during sample preparation and were excluded in the subsequent analyses. CapEC was the major constitutions of ECs in GA muscles of both mouse genotypes post ischemia and in comparison with *Pparδ*$^{EC\text{-}KO}$ mice, there were more capECs in *Pparδ*$^{EC\text{-}WT}$ mice (86.37% vs 53.89%). By contrast, the proportions of EC1 and EC2 were higher in *Pparδ*$^{EC\text{-}KO}$ mice (Fig. 1e, Fig. S1b). EC1 only appeared in the *Pparδ*$^{EC\text{-}KO}$ sample (727/3585), but not in the *Pparδ*$^{EC\text{-}WT}$ (0/6563). In addition, less significant change of

venous ECs (vECs) (around 6.3%) and aECs (around 2.7%) were observed in both genotypes (Fig. 1e). To discriminate more ambiguous populations, we performed differential gene expression (DEG) analysis between clusters and all other cells in the atlas, which demonstrated the distinct DEG signature (Fig. 1f).

3.2. Deletion of endothelial PPARδ alters EC expression profile in EC subclusters after HLI

To further identify EC signaling and phenotype altered by PPARδ deletion, we then analyzed DEGs, followed by pathway analysis using DEGs, focusing on the 4 major EC clusters capEC, aEC, vEC, and EC2 that were commonly appeared in *Ppard*$^{EC\text{-}KO}$ and *Ppard*$^{EC\text{-}WT}$ mice. Herein, DEGs were calculated by natural log(fold change) (lnFC) for *Ppard*$^{EC\text{-}KO}$ relative to *Ppard*$^{EC\text{-}WT}$ in each EC cluster and were considered significant if reaching statistical significance, i.e., (FDR-adjusted *P*-value <0.05) with $|\log2(FC)| > 0.5$. Overall, for both genotypes, EC2, vEC and capEC had almost equivalent number of changed genes, and more than the aEC (Fig. S2a). In comparison with *Ppard*$^{EC\text{-}KO}$, every EC cluster of *Ppard*$^{EC\text{-}WT}$ ischemic muscle had more upregulated genes (Fig. S2a), suggesting PPARδ potentially influences gene expression of each EC subtype in ischemic muscle. Interestingly, aEC, vEC and capEC had their unique DEGs, while EC2 did not have (Fig. S2b, red rectangle). Further, by overlapping analysis of unique DEGs between any two or three clusters, vEC/capEC and vEC/capEC/aEC had the most number (7 and 6 unique DEGs), whereas EC2 together with other one or two clusters showed the least (Fig. S2b , blue and green rectangle). Specifically, three DEGs existed in all EC subtypes (Fig. S2b), they are *Sox18*, *Serpinh1*, *Hspa5,* all of which were upregulated in ischemic muscle of *Ppard*$^{EC\text{-}KO}$. These results indicated heterogeneous regulations of different EC population by PPARδ in the hindlimb ischemic muscle.

To further identify EC signaling and phenotype altered by PPARδ, we performed pathway analysis using DEGs focusing the 4 major EC clusters capEC, aEC, vEC, and EC2. EC1 was not included because it only appeared in *Ppard*$^{EC\text{-}KO}$ mice and we will describe this particular part of the data separately below. This pathway analysis identified several signaling pathways functionally associated with HLI including: angiogenesis, hypoxia signaling, alternation of cellular junctions, immune responses, eNOS and VEGF signaling, oxidative stress responses, etc. (Fig. 2a). It is also expected to observe changes in mitochondrial metabolism which is a well-defined function of PPARδ. A more detailed GSEA analysis of gene function in Fig. 2b showed for example upregulation of many pathways in immune response most significantly in the aEC cluster from *Ppard*$^{EC\text{-}KO}$ mice (Fig. 2b). Despite unique change in one sub-cluster, there are also some pathways were altered similarly in all 4 clusters for example metabolism and cell proliferation (Fig. 2b). These changes indicated both common and unique responses of various EC clusters regulated by PPARδ.

Next, we looked into individual DEGs which are grouped into 4 EC functional pathways (Fig. 2c) identified from Fig. 2b. We observed that genes related to angiogenesis were increased mostly in wild type capECs, such as *Flt1* and *Klf2* (Fig. 2c). In addition, capEC number was less in the *Ppard*$^{EC\text{-}KO}$ mice (Fig. 1e), indicating possibly an impaired angiogenesis. More upregulations were also detected with inflammatory responses in the capEC of *Ppard*$^{EC\text{-}KO}$ mice (Fig. 2c), such as *Icam1* and *Ctsb*, indicating more vascular inflammation, which was further supported by upregulation of genes involved in cell adhesion, mostly in the capEC and vEC of *Ppard*$^{EC\text{-}KO}$ mice (Fig. 2c). Conversely, more upregulation of junctional proteins was found in the wild type capEC (Fig. 2c), indicating better recovery of endothelial barrier in *Ppard*$^{EC\text{-}WT}$ mice. Of note, few changes except genes involved in cell proliferation, were found in the EC2 cluster (Fig. 2b).

Interestingly, a unique EC1 cluster only appeared in *Ppard*$^{EC\text{-}KO}$ mice (Fig. 1e, Fig. S1b). Most of the EC1 cells (~75%) expressed *Cdh5* and *Pecam1*, indicating their EC identity (Fig. S1c, S1d). However, when compared with other clusters, many of the EC1 cells (>30%) also expressed fibroblast or myofibroblast markers such as *Acta2*, *Col1a1* and *Col1a2*, making them somewhat similar to fibroblast and smooth muscle cells (Fig. 1d). Examples of most significant DEGs in EC1 cluster, such as *Col3a1*(encoding collagen III) and *Cd63* (Fig. S2c, S2d) could be found to be upregulated in the capECs from *Ppard*$^{EC\text{-}KO}$ (Fig. S2c, S2d), indicating that EC1 might be derived from capEC. The gene network analysis (Fig. 2d) showed that many genes in EC1 are involved in transmitting extracellular signals to surface receptors on EC, and further triggering downstream signaling involved in both pro-fibrotic and pro-inflammatory changes. Several DEGs in EC1 including *Col3a1*, *Lgals1* (Galectin-1), involved in vascular fibrosis were altered, as well as several DEGs including *Ctsb* (Cathepsin B), *Hspa5* (BiP), *Anxa1/5*, *Cnbp* involved in inflammatory responses (Fig. 2c). Therefore, EC1 might represent ECs mal-adapting to the angiogenic signals, which instead, triggers pro-fibrotic and pro-inflammatory responses in ECs, such as endothelial to mesenchymal transition (EndoMT). Collectively, these results suggest that endothelial PPARδ is protective for vascular remodeling and its loss is detrimental for post-ischemic vascular repair.

3.3. Endothelial PPARδ knockout impairs angiogenesis, endothelial tight junction and facilitates inflammation

Next, we confirmed endothelial localization and expression pattern for several key DEGs. Immunofluorescence staining validated the downregulations of junctional protein claudin-5 (*Cldn5*, Fig. 3a), and regulator of angiogenesis VEGFR1 (*Flt1*, Fig. 3b); and the upregulations of CD63 (implicated in leukocyte recruitment, Fig. 3c), and also CD81 (implicated in cell migration, Fig. 3d), in the 7-day ischemic muscles after PPARδ knockout in ECs. Further validation performed by qPCR showed significant downregulation of these DEGs in ECs isolated from injured hindlimb muscle of *Ppard*$^{EC\text{-}KO}$ mice, implicating dysregulation including increased endothelial activation, increased leukocyte adhesion and transmigration and inflammation response (Fig. 3e, f), with inhibition of both tight junction (Fig. 3f) and adherens junctions (Fig. 3g). Altogether, these results support the scRNA-seq data indicating that loss of PPARδ induced dysregulation in many different aspects of EC function and phenotype including angiogenesis, cell junction, adhesion, migration, etc.

3.4. Re-expressing endothelium-targeted PPARδ restores endothelial function after HLI

Our single-cell RNA-seq revealed a key regulatory role for endothelial PPARδ in a model of hindlimb ischemia. Importantly, strikingly downregulated expression level of *Ppard* was observed in endothelial cells isolated from ischemia muscles (Fig. 4a, b). Given that PPARδ has the ligand-independent roles in endothelial homeostasis [28], we thus asked whether restoring the expression of endothelial PPARδ would ameliorate endothelial dysfunction and enhance vascular repair in the HLI mouse model.

ICAM-2 is a cell surface adhesion molecule constitutively expressed in vasculature endothelial cells and megakaryocytes and ICAM2 promoter driving overexpression of targeted genes in ECs was successfully achieved by adeno-associated virus AAV1 [11,37]. Our scRNA-seq data also validated the abundant expression of ICAM2 in clusters of endothelial cells (Fig. S3a). Therefore, we followed the methodology [46] and transduced mouse *Ppard* expression by AAV-*Ppard*, i.e., ICAM2-driven mouse *Ppard* expression by AAV1. Both *Ppard*$^{EC\text{-}WT}$ and *Ppard*$^{EC\text{-}KO}$ mice were used for intramuscular injection at a single dose of 1×10^{11} vg/mouse of AAV1- ICAM2-*Ppard* (AAV-*Ppard*) and AAV1-ICAM2 (as negative control, AAV-control) 7 days before performing common iliac artery ligation, to examine the efficacy of restoring *Ppard* to enhance vascular repair.

At 28 days after AAV injection, upregulation of PPARδ could be observed in the GA muscles of both genotypes when compared to the AAV-control (Fig. S3b). Consistently, immunofluorescence staining of

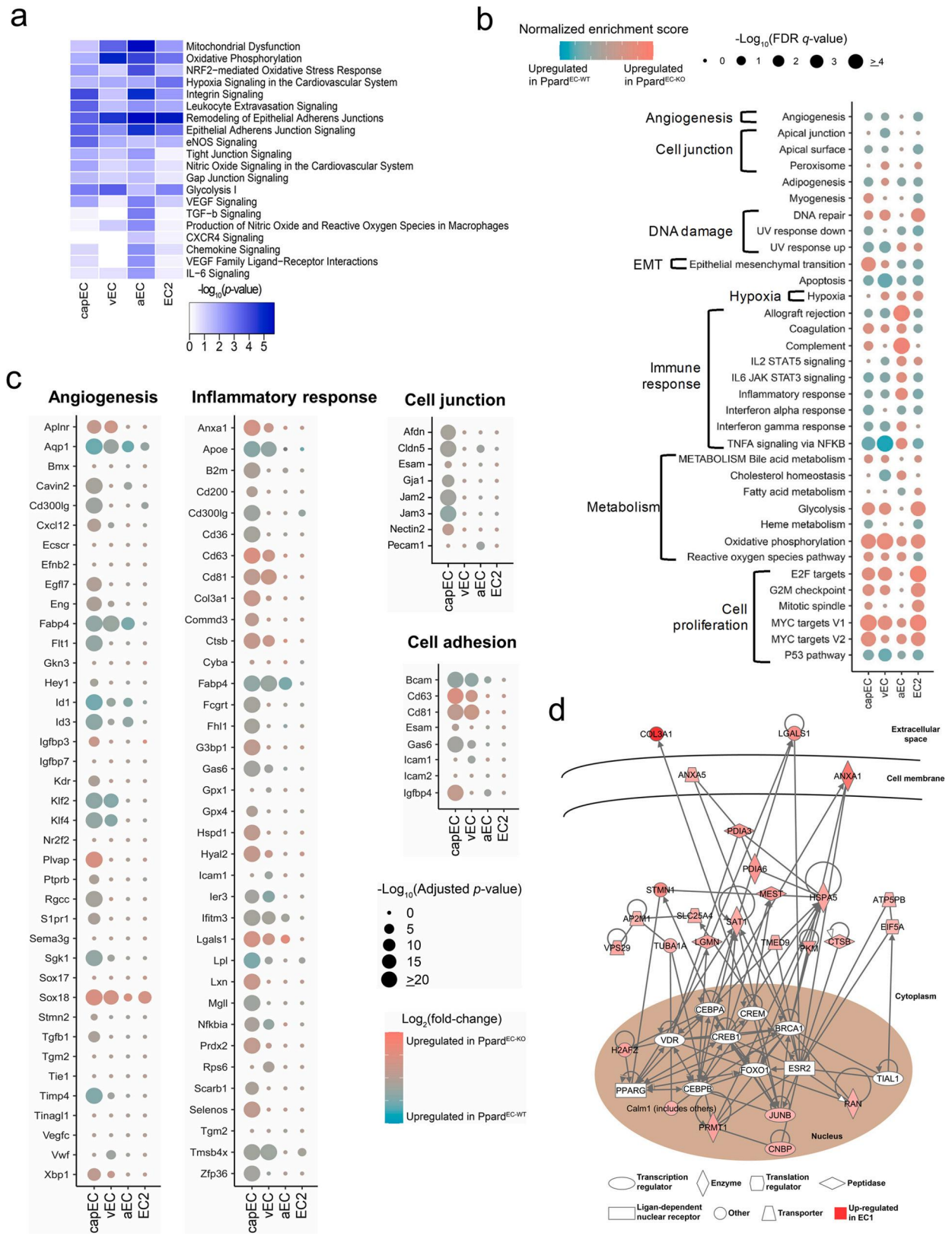

Fig. 2. Endothelial *Ppard* knockout compromises the recovery of vascular homeostasis after HLI. (a) Heatmap showing the significantly changed canonical pathways (–log10 (p-value))analyzed by Ingenuity Pathway Analysis (IPA) using DEGs for four EC subtypes. (b) Dot plot showing the enrichment of pathways obtained from the gene set enrichment analysis (GSEA) by using the Molecular Signatures Database hallmark gene set collection, normalized enrichment score (color) and –log10 (FDR q-value) (radius). (c) Dot plots showing the expression change of representative genes in indicated enriched pathways, log2 (fold-change) (color) and –log10 (adjusted p-value) (radius). (d) IPA analysis showing the gene regulatory network of EC1 cluster distinctly appeared in *Ppard*$^{EC\text{-}KO}$ mice.

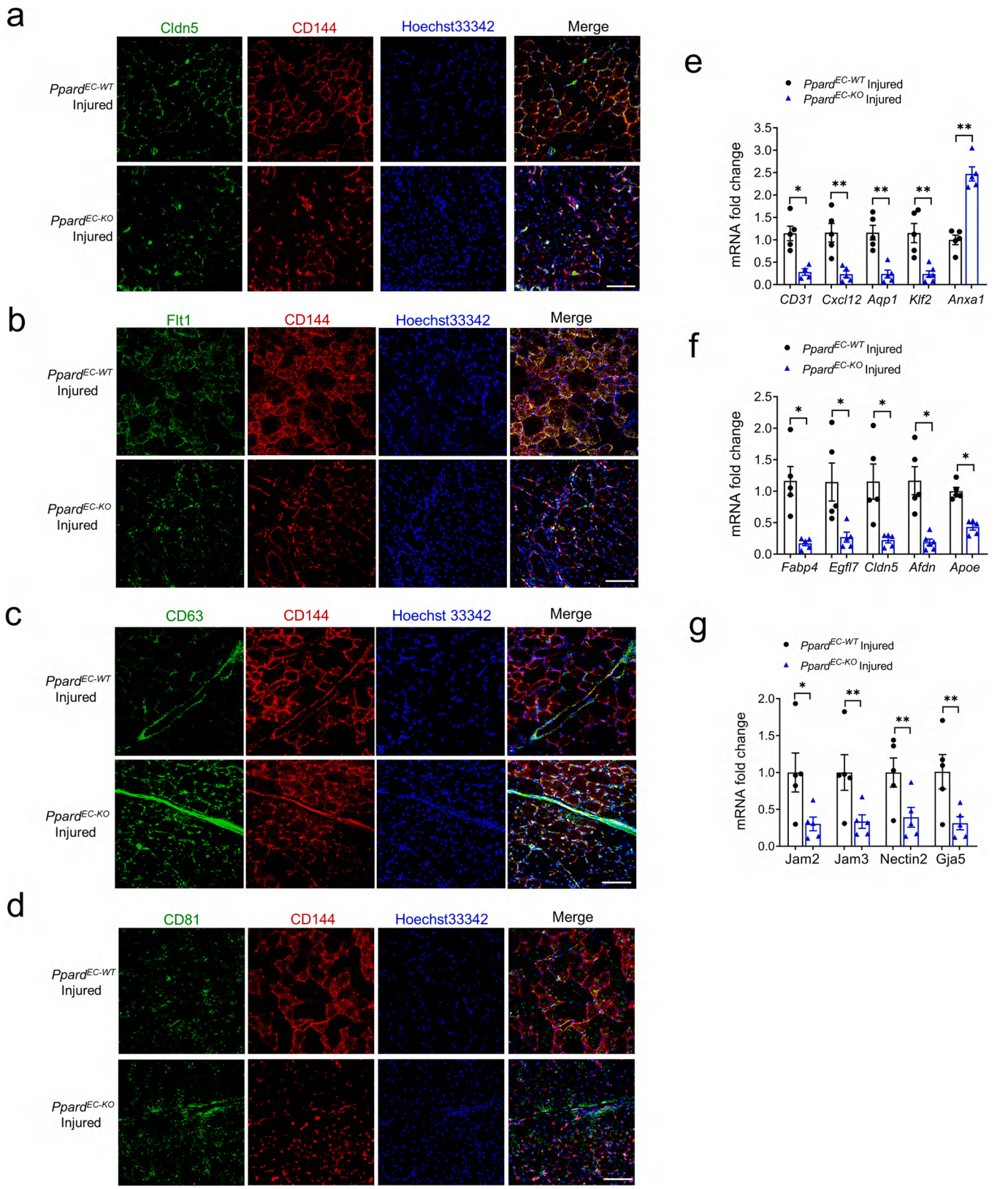

Fig. 3. Endothelial *Ppard* knockout impairs angiogenesis, endothelial tight junction and facilitates inflammation. (a-d) Representative images showing the immunofluorescent staining of indicated markers in muscle sections from the $Ppard^{EC\text{-}WT}$ and $Ppard^{EC\text{-}KO}$ mice post HLI on day 7. (a) Cldn5 or claudin-5, (b) Flt1 or VEGFR1, (c) CD63 or LAMP-3, (d) CD81: Representative separated single-color images of immunofluorescence of the same markers, CD144 marked endothelial cells, Hoechst 33342 indicated nucleus. (n = 5, each group). Scale bar: 200 μm. (e-g), Validation of DEGs using ECs isolated from injured muscle of both genotypes (n = 5, each group). * $p < 0.05$, * * $p < 0.01$ between groups by two-tailed Student's t-test.

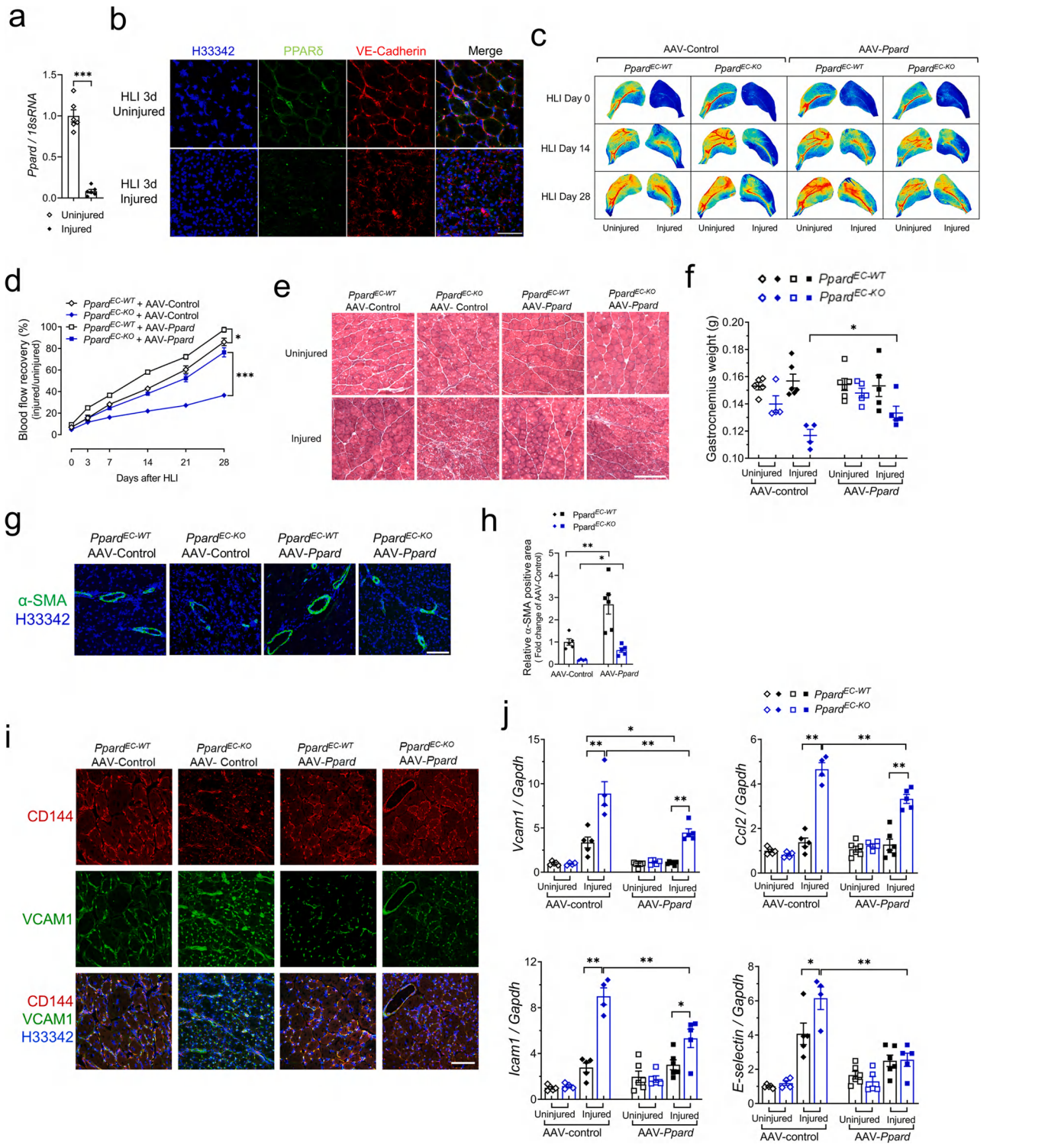

Fig. 4. Restoration of endothelial PPARδ expression ameliorates vascular functions in *Ppard*$^{EC\text{-}KO}$ mice post HLI. (a) Quantitative PCR analysis of *Ppard* mRNA expression in endothelial cells isolated from uninjured and injured skeletal muscles of wildtype mice post HLI after 3 days (n = 5 and 6, each group). (b) Representative images of immunofluorescent staining showing PPARδprotein expression levels in indicated muscles; VE-cadherin, marking endothelial cells; (n = 5–6, each group). (c, d) Representative images (c) and related statistical analyzes (d) showing the blood flow recovery in muscles of *Ppard*$^{EC\text{-}WT}$ and *Ppard*$^{EC\text{-}KO}$ mice post HLI, with injection of AAV-control or AAV-*Ppard*. Left uninjured controlled legs; right, injured legs. * $p < 0.05$, * * $p < 0.01$, * ** $p < 0.001$ between groups by one-way ANOVA and multiple comparison test. (e) Representative images displaying H&E staining of muscles at day 28 after HLI (n = 5–6, each group). Scale bars: 200 μm. (f) Measurement of GA Muscle weight derived from mice with indicated treatment in (c) (n = 5–6, each group). (g) Representative images showing the positive arterioles by immunofluorescent staining of α-smooth muscle actin (α-SMA) in ischemic muscles of *Ppard*$^{EC\text{-}WT}$ and *Ppard*$^{EC\text{-}KO}$ mice at day 28 after HLI with indicated AAV1 injection (n = 5–6, each group). Scale bars: 200 μm. (h) Quantification of α-SMA marked positive arterioles in (g) (n = 5–6, each group). (i) Representative images showing the immunofluorescent staining of VCAM1 (indicate endothelial cell inflammation) and CD144 (mark endothelial cells) in muscle sections of indicated mice (n = 5–6, each group). Scale bars: 200 μm. (j) Quantitative PCR analysis of inflammatory genes in samples derived from GA muscles of mice with related treatment. Bars, means ± SEM; * $p < 0.05$, * * $p < 0.01$, calculated between groups by one-way ANOVA and multiple comparison test.

PPARδ co-expressed with VE-Cadherin in the muscles of *Ppard*$^{EC\text{-}WT}$ mice after AAV-*Ppard* injection confirmed the successful gene delivery by this strategy (Fig. S3c). AAV-*Ppard* accelerated perfusion recovery in the hindlimb in *Ppard*$^{EC\text{-}WT}$ mice, and also restored the impaired recovery in *Ppard*$^{EC\text{-}KO}$ mice (Fig. 4c, d). Further histological analysis showed that AAV-*Ppard* resulted in better recovery after muscle damage and less fibrosis (Fig. 4e), as well as less GA muscle mass reduction (Fig. 4f), which was more obvious in AAV-*Ppard* injected *Ppard*$^{EC\text{-}KO}$ mice.

We then examined the effect of PPARδ on blood vessel formation by measuring the blood vessel density using α-SMA as marker for arterioles. As shown, after HLI injury, AAV-*Ppard* injection increased the area of positive arterioles in both of *Ppard*$^{EC\text{-}WT}$ (169% increase vs control) and *Ppard*$^{EC\text{-}KO}$ mice (230% increase vs control) in comparison with the

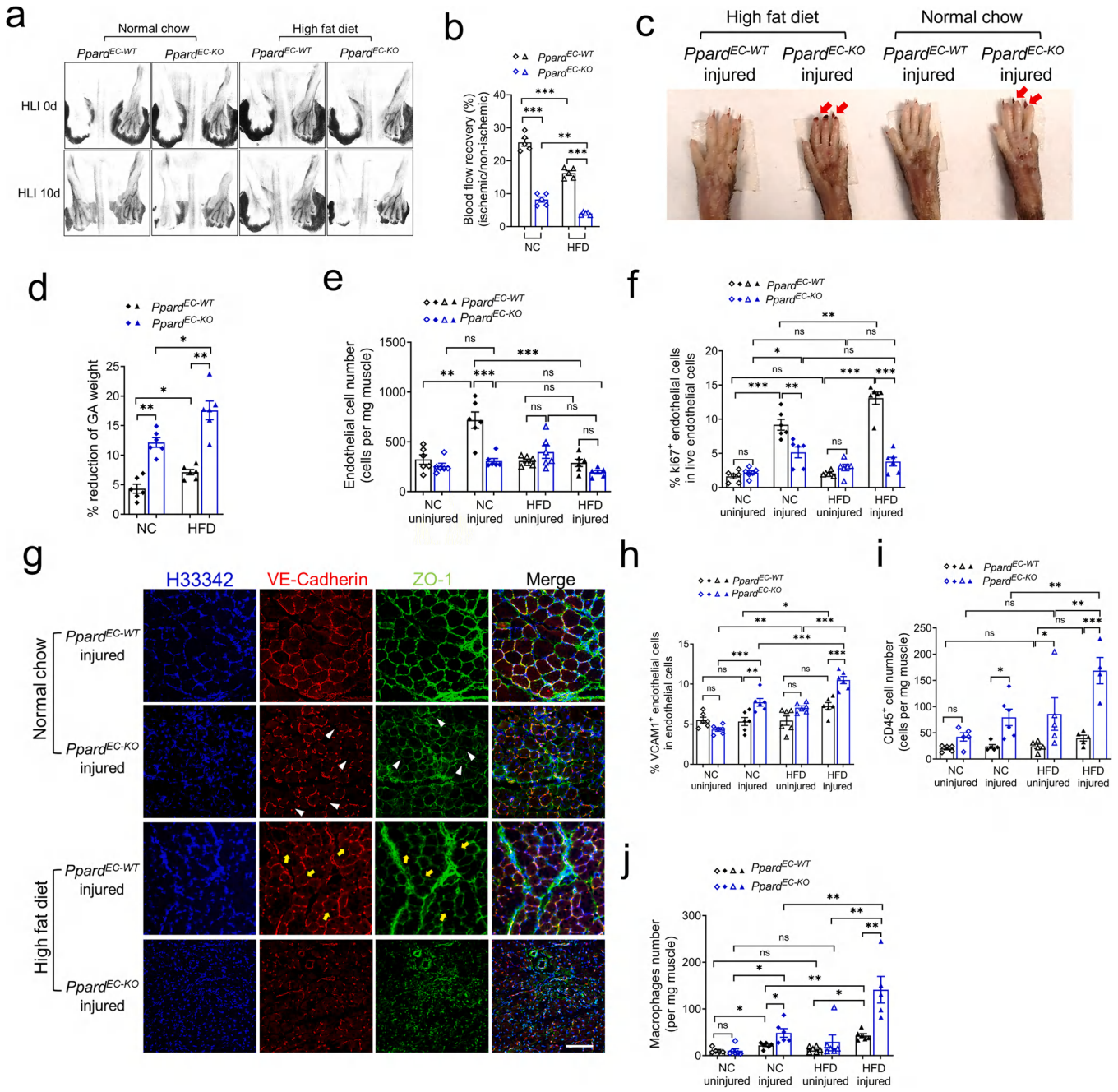

Fig. 5. *PPARδ* deficiency facilitates angiogenic dysfunctions in high fat diet induced obese mice. (a, b) Representative images (a) and related statistical analyzes (b) showing the blood recovery of mouse foot area recorded at day 10 after HLI in *Ppard*$^{EC\text{-}WT}$ and *Ppard*$^{EC\text{-}KO}$ mice with HFD treatment or not (n = 6, each group). Left legs, injured by HLI; right legs, normal. (c) Representative pictures showing the foot color and nails of indicated mice at day 10 after HLI. Red arrow, necrosis nails. (d) Measurement of GA muscle weight in mice with indicated treatment at day 10 after HLI (n = 6, each group). (e) Flow cytometric analysis of CD45$^-$CD144$^+$ ECs at day 10 after HLI. (f) The bars showing the percentage of proliferating ECs by flow cytometric analysis of CD45$^-$CD144$^+$Ki67$^+$ ECs at day 10 after HLI. (g) Representative images showing the immunofluorescent staining of ZO-1 and VE-Cadherin in GA muscles of indicated mice at day 10 after HLI (n = 6, each group). Scale bar: 200 μm. White Triangle, continuous endothelium, yellow arrowhead, discontinuous endothelium. (h-j) Charts showing the flow cytometric analysis of the percentage of CD45$^-$CD144$^+$VCAM1$^+$ ECs in total ECs (h) infiltrated CD45$^+$ leukocytes (i) and infiltrated CD11b$^+$Ly6C$^-$CD64$^+$ macrophages (j) in GA muscles of indicated genotypic mice at day 10 after HLI. Bars, means ± SEM; * $p < 0.05$, * * $p < 0.01$, * ** $p < 0.001$ calculated between groups by one-way ANOVA and multiple comparison test.

AAV-Control at days 28 post HLI (Fig. 4g, h). We also test some important factors involved in endothelial integrity. The expression of CD144 increased after AAV-*Ppard* injection in the $Ppard^{EC\text{-}KO}$ mice, and more importantly, the pattern of CD144 was more continuous in the capillaries indicating a restoration of functional endothelium after re-expression of PPARδ in the $Ppard^{EC\text{-}KO}$ mice (Fig. 4i). The high expression of VCAM1, a marker for vascular inflammation, was attenuated in the $Ppard^{EC\text{-}KO}$ mice after AAV-*Ppard* injection (Fig. 4i, j). In addition, qPCR results showed that the high expressions of adhesion molecules *Icam1* and *Sele* (E-selectin), and chemokine *Ccl2*, as markers for endothelial activation, were attenuated by AAV-*Ppard* in the $Ppard^{EC\text{-}KO}$ mice (Fig. 4j), whereas the effect was less obvious in the $Ppard^{EC\text{-}WT}$ mice, probably because at this time point the vascular inflammation was already resolved.

3.5. High fat diet suppresses PPARδ expression and exacerbates vascular injury after HLI

Obesity and insulin resistance is associated with PAD and especially CLI, with almost 1.5 times more risk to develop CLI compared to normal weight population [7]. Given that endothelial PPARδ is crucial for vascular repair post HLI, we asked whether endothelial PPARδ inhibition contributed to the more severe injury for the obese-related PAD. We firstly fed mice from 8 weeks old with the high fat diet (HFD) to induce obesity and insulin resistance for 12 weeks. After HFD feeding, the fasting glucose and body weight were higher in the HFD group (Fig. S4a, S4b). In addition, the fasting glucose was higher in the HFD-fed $Ppard^{EC\text{-}KO}$ mice than their wild type littermates (Fig. S4a). Increase of adiposity due to HFD feeding were also similar between genotypes (Fig. S4c), while no difference in the heart/body weight ratio in two genotypes of normal chow (NC)- and HFD-fed mice (Fig. S4d). Overall, not many apparent differences were observed between HFD-fed $Ppard^{EC\text{-}WT}$ and $Ppard^{EC\text{-}KO}$ mice if without further treatment. We then manipulated them with HLI. As shown in Fig. 5a, b, HFD further delayed perfusion recovery of $Ppard^{EC\text{-}KO}$ mice than NC fed $Ppard^{EC\text{-}KO}$. Additionally, on day 10 after HLI, compared with the $Ppard^{EC\text{-}WT}$, worse necrotic damage was visible in the injured HFD fed $Ppard^{EC\text{-}KO}$ mice than NC-fed mice (Fig. 5c). The reduction of muscle mass of GA muscle after injury was observed in both NC and HFD fed $Ppard^{EC\text{-}KO}$ mice, which was more in the HFD fed group (Fig. 5d). Similar and more obvious decrease of tibialis anterior (TA) muscle mass was also observed in HFD $Ppard^{EC\text{-}KO}$ mice (Fig. S4e). These results suggest that loss of endothelial PPARδ further compromise muscle repair after HLI in mice with obesity and insulin resistance.

We then examined the change of EC phenotype. By flow cytometric analysis of $CD45^{-}CD144^{+}$ ECs, NC fed wild type mice had more EC compared with NC fed $Ppard^{EC\text{-}KO}$ mice, suggesting normal angiogenesis and/or less vascular injury and cell death (Fig. 5e). Similar EC numbers were detected regardless of genotype of HFD fed mice, while HFD fed $Ppard^{EC\text{-}KO}$ mice had the least amount of EC, suggesting that both HFD and deletion of PPARδ impaired vascular repair (Fig. 5e). Consistently, the Ki67 staining of proliferating ECs was significantly less in the injured muscle of both NC and HFD fed $Ppard^{EC\text{-}KO}$ mice, compared to their wild type littermates, while HFD did not show reduction of EC proliferation compared to NC fed $Ppard^{EC\text{-}WT}$ mice (Fig. 5f). These results suggest that HFD and inhibition of PPARδ impairs vascular repair potentially through both common and distinct cellular mechanisms. We also characterized endothelial integrity by examining VE-cadherin, and the tight junction protein ZO-1, which regulates tension acting on VE-Cadherin-based adherens junctions, cell migration, and barrier formation of endothelial cells, as well as angiogenesis [47]. In the $Ppard^{EC\text{-}WT}$ mice at day 10 after HLI, HFD resulted in a discontinuous expression of both VE-cadherin and ZO-1 most likely in the newly emerged capillaries (Fig. 5g, the first vs third row, indicated by yellow arrowheads), such discontinuous pattern was more apparently observed in the NC-fed $Ppard^{EC\text{-}KO}$ mice (Fig. 5g, the second group of images, indicated by white triangles). Notably, continuous capillary was scarce in the muscles of HFD-treated $Ppard^{EC\text{-}KO}$ mice (Fig. 5g, the fourth group of images), indicating that HFD disrupts endothelial integrity and PPARδ has potential protective roles.

VCAM-1 is identified as an endothelial cell surface glycoprotein, which is induced by pro-inflammatory cytokines [48]. Flow cytometry analysis of VCAM1 expression on ECs showed that ischemic injury induced more persistent upregulation of VCAM1 in the $Ppard^{EC\text{-}KO}$ mice from both NC and HFD, whereas HFD induced an insignificant increase of VCAM1 expression on ECs from the uninjured $Ppard^{EC\text{-}KO}$ mice as well (Fig. 5h). Importantly, HFD treatment enhanced VCAM1 expression after injury in the $Ppard^{EC\text{-}KO}$ mice. We then analyzed leukocyte infiltration, and more specifically, macrophage infiltration, as a response to VCAM1 expression. The cell number quantification showed that ischemic injury increased both $CD45^{+}$ leukocyte and $CD11b^{+}Ly6C^{-}CD64^{+}$ macrophage infiltration in the injured muscle, which was exacerbated in both NC and HFD-fed $Ppard^{EC\text{-}KO}$ mice (Fig. 5i, j). HFD only enhanced immune cell infiltration in $Ppard^{EC\text{-}KO}$ mice but not in wild type, suggesting that deletion of PPARδ sensitized ECs to more severe inflammation after ischemic injury (Fig. 5i).

Interestingly, the number of infiltrated $CD45^{+}$ leukocytes and $CD11b^{+}Ly6C^{-}CD64^{+}$ macrophage increased in injured muscles of both NC and HFD-fed $Ppard^{EC\text{-}KO}$ mice at 10 days after ischemia, with more increase in HFD fed mice (Fig. 5i, j, Fig. S4f). This is in line with the increased expression of VCAM1 on ECs which stimulated leukocyte infiltration [49]. In summary, our results report that PPARδ loss would exacerbate the HFD induced vascular dysfunctions in ischemia disease by decreasing proliferating ECs, disrupting EC integrity and aggregating the regional pro-inflammatory immune environment.

3.6. Gene therapy by delivery of endothelial PPARδ improves vascular repair in HFD-induced obese mice after HLI

Our results showed delayed vascular repair in $Ppard^{EC\text{-}KO}$ mice and downregulation of endothelial PPARδ expression in ECs when suffered ischemia injury. In addition, restoring endothelial PPARδ expression promoted blood flow recovery by restoring endothelial function and inhibiting endothelial inflammation, suggesting that endothelial PPARδ might be a feasible target for gene delivery in experimental CLI. More interestingly, after 3 months fed with HFD, mRNA level of PPARδ in skeletal muscle was significantly decreased (Fig. 6a). We therefore tested whether overexpression of endothelium-targeted PPARδ improved vascular repair after hindlimb ischemia in obese and diabetic mice, using AAV1 which carried ICAM2 to drive PPARδ expression (AAV-*Ppard*), as aforementioned. C57BL/6 mice under 12-weeks HFD were intramuscularly injected with AAV-ICAM2-*Ppard* (AAV-*Ppard*) and the empty vector as control (AAV-Control) 7 days in advance before inducing ischemic. Blood flow in HFD mice after ligation re-appeared later than NC fed mice (Fig. 6b, c, compared with results from Fig. 4d). In addition, the recovery was significantly better with AAV-*Ppard* (52.3%) vs AAV-control (27.4%) (Fig. 6c). Accordingly, improving blood flow recovery was associated with a markedly decreased number of necrotic toes in mice treated by AAV-*Ppard* (Fig. 6d). In addition, no significant change of body weight and heart/body weight ratio in both groups (Fig. S5a, S5b).

Furthermore, ischemia induced loss of GA and TA muscle was apparent in mice with AAV-Control, while AAV-*Ppard* treatment counteracted such effect and restored muscle mass similar to normal levels (Fig. 6e, f). Histological analysis of GA muscles also showed less severe muscle degeneration and muscle fiber apoptosis, accompanied by less immune cell infiltration in AAV-*Ppard* treated mice, suggesting that AAV-*Ppard* suppressed ischemia induced muscle damage, indicated by H&E staining and Masson's Trichrome staining, respectively (Fig. 6g, h). Moreover, the better muscle repair in AAV-*Ppard* group was also evident in the gene expression profile showing more upregulation of muscle progenitor markers *Pax3* and *Pax7*, and early myogenic markers *Myf5*,

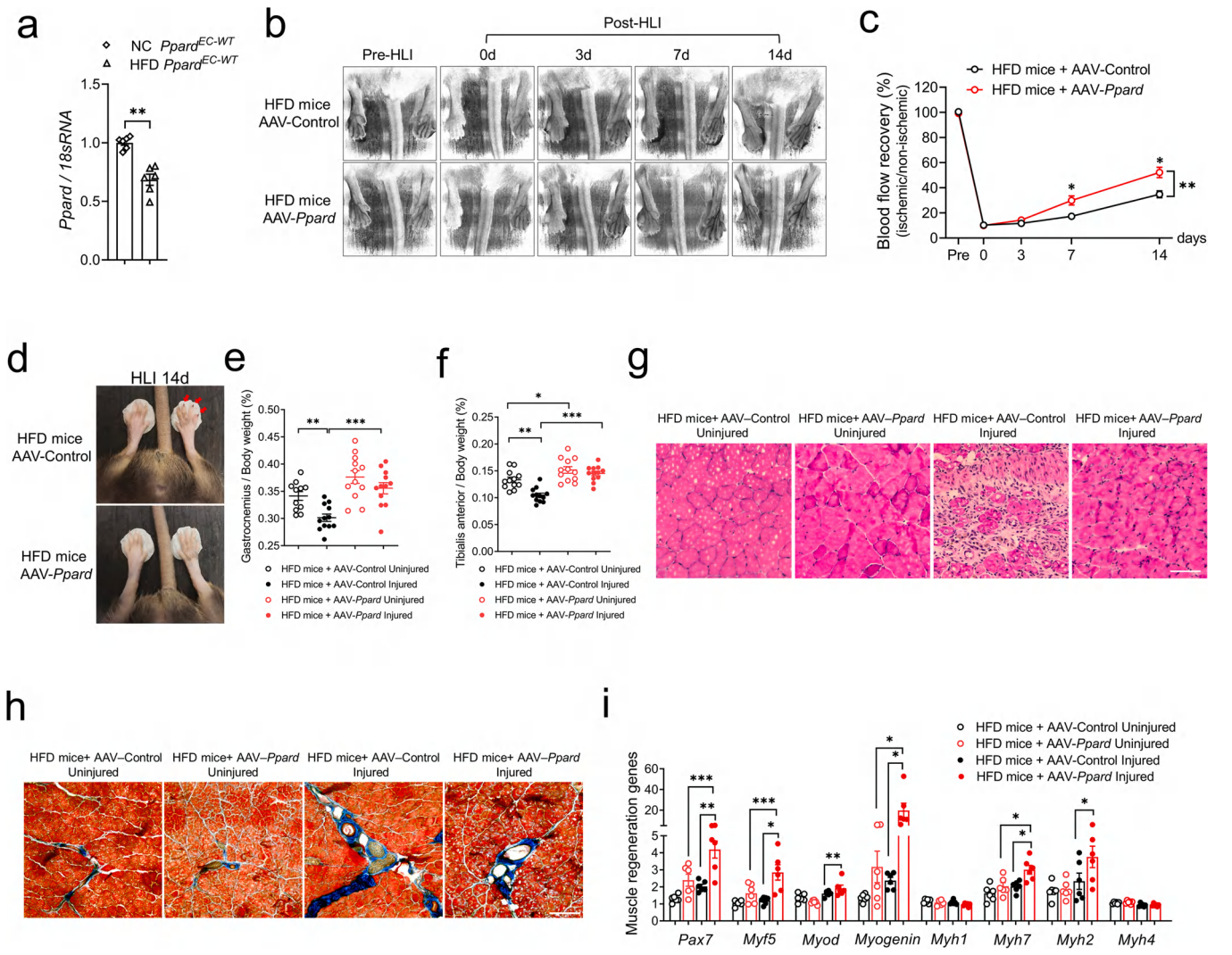

Fig. 6. Gene therapy mediated by delivery of endothelial AAV1-*Ppard* improves muscle regeneration in high-fat diet-induced obese mice after HLI. (a) Quantitative PCR analysis of *Ppard* levels in skeletal muscles of mice with or without HFD treatment. (b, c) Representative images (b) and related statistical data (c) showing the blood recovery of mouse foot area in mice with indicated treatment. Left leg, injured; right leg, uninjured (n = 11–12, each group). (d) Representative pictures of the foot color and nails at days 14 after HLI. Red arrow, necrosis nails. (e, f) Measurement of GA and TA Muscle weight at day 14 after HLI (n = 11–12, each group). (g) Representative images of H&E staining analyzing uninjured and injured GA muscles in mice with indicated AAV injection at day 14 after HLI (n = 5–6, each group). Scale bars: 200 μm. (h) Representative images showing the Masson trichrome staining analysis of uninjured and injured muscles in (f) at day 14 after HLI (n = 5–6, each group). Scale bars: 200 μm. (i) Quantitative PCR analysis of gene expression related to muscle regeneration in samples derived from mice in (g) (n = 6, each group). Bars, means ± SEM; * $p < 0.05$, * * $p < 0.01$, * ** $p < 0.001$, calculated between groups by one-way ANOVA and multiple comparison test.

Myod1, and *Myog* in the AAV-*Ppard* group (Fig. 6i). These results underline that endothelium-targeted delivery to express PPARδ is effective to improve vascular repair particularly in the context of obesity and insulin resistance.

Next, we examined vascular structure and function improved by AAV-*Ppard*. Flow cytometric analysis showed more EC number in the injured muscle from AAV-*Ppard* (Fig. 7a), which was probably due to more proliferation of ECs indicted by Ki67 staining (Fig. 7b). In addition, further upregulation of many angiogenic factors such as *Vegfr2*, *Pdgfb*, *α-SMA*, and *Apelin* was also observed with AAV-*Ppard* after injury (Fig. 7c), indicating that AAV-*Ppard* enhanced post-ischemic angiogenesis. Furthermore, the improvement of endothelial integrity was also observed with AAV-*Ppard*, indicated by upregulation of genes related to endothelial junction, including *Cldn5*, *Cdh5* and *Tjp1* (Fig. 7d). Improved endothelial barrier function was also accompanied by less inflammatory responses, reflected by less expression of adhesion molecule VCAM1 on ECs from muscles of AAV-*Ppard* (Fig. 7e), as well as *Icam1*, *Ccl2*, and *E-selectin* (Fig. 7f). Accordingly, less T lymphocyte infiltration was observed in the injured muscle from AAV-*Ppard* group (Fig. 7g). Lastly, as shown by immunofluorescence staining for α-SMA and VEGFR2, although not much difference was observed with VEGFR2 expression level and morphology, the induction of newly formed arterioles labeled by α-SMA was improved by AAV-*Ppard* (Fig. 7h). These results supported that endothelium-targeted overexpression of PPARδ promotes blood reperfusion after ischemia, and facilitates muscle repair, by enhancing the restoration of endothelial homeostasis.

4. Discussion

Our study tested whether targeting endothelial PPARδ is effective to improve the outcomes of vascular repair in experimental CLI model. Using AAV vector to selectively express PPARδ in ECs, we showed that PPARδ was able to improve revascularization, to resolve inflammatory response and to promote muscle regeneration in both normal and HFD-induced obesity mice.

We first used scRNA-seq of ECs from ischemic muscle to show that

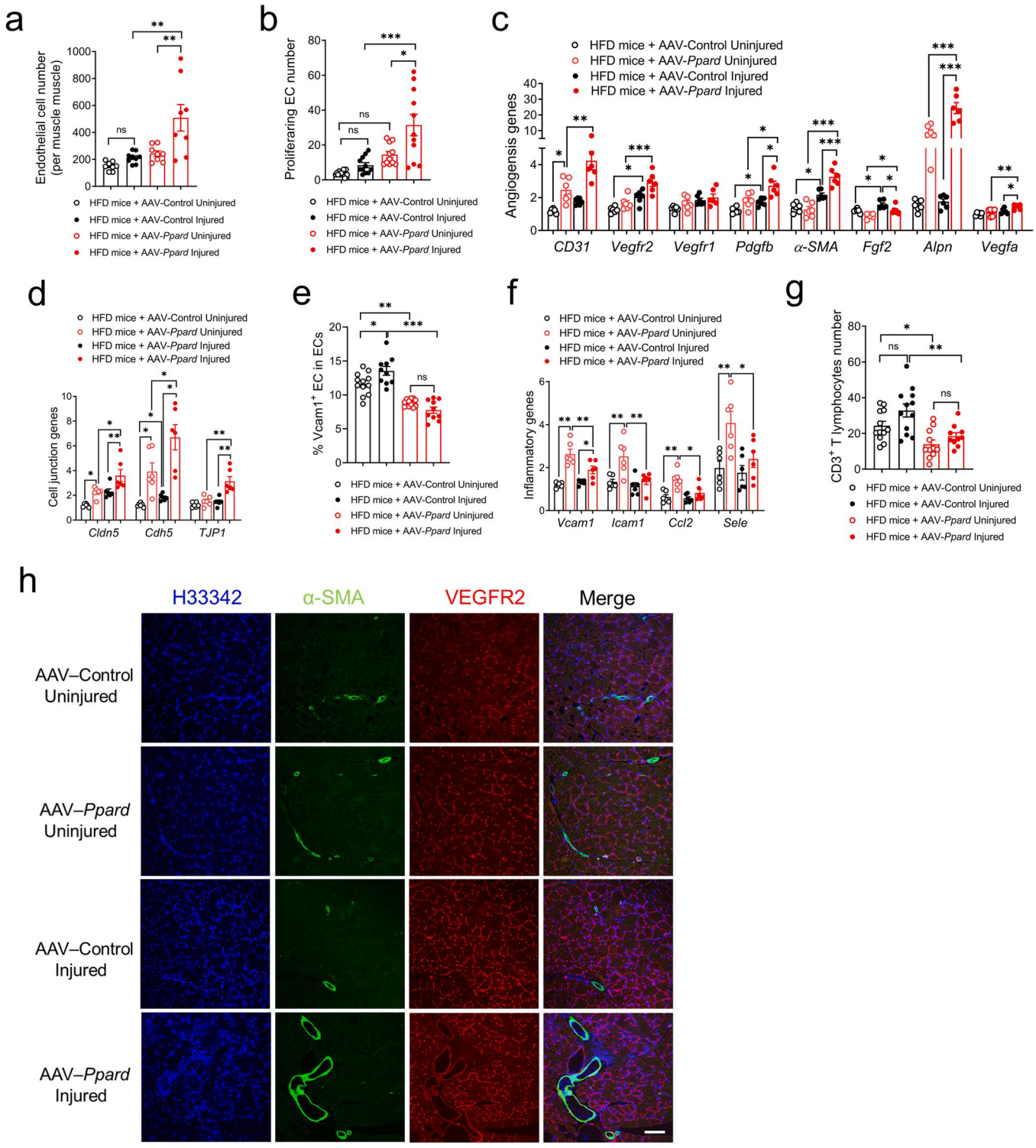

Fig. 7. Gene therapy mediated by delivery of endothelial AAV1-*Ppard* rescues vascular functions in high-fat diet-induced obese mice. (a, b) Flow cytometric analysis of $CD45^{-}CD144^{+}$ total ECs (a) and $CD45^{-}CD144^{+}Ki67^{+}$ proliferating ECs in GA muscles of mice with indicated treatment at day 14 after HLI. (c, d) Quantitative PCR analysis of angiogenesis and endothelial junction related gene expression in samples derived from (a) (n = 6, each group). (e, g) Charts showing the flow cytometric analysis of percentage of $CD45^{-}CD144^{+}VCAM1^{+}$ ECs (e), and $CD3^{+}$ T lymphocytes (g) in relevant GA muscles of mice at day 14 after HLI. (f) Quantitative PCR analysis of vascular inflammation-related gene expression in samples collected from mice in (e) (n = 6, each group). (h) Representative images of immunofluorescent staining of α-SMA and VEGFR2 in muscles of mice with indicated treatment at day 14 after HLI (n = 6, each group). Scale bars: 200 μm. Bars, means ± SEM; * $p < 0.05$, * * $p < 0.01$, * ** $p < 0.001$, calculated between groups by one-way ANOVA and multiple comparison test.

PPARδ orchestrates many functional aspects of ECs including angiogenesis, vasodilatation, vascular barrier function, and inflammatory responses. We identified 5 major EC clusters with different cell numbers of each genotype, with more obvious change in capECs, which strongly suggest the association of hypoxia signaling and several pathways related to EC function. Apart from the known target genes of PPARδ, we also found several previously unidentified EC enriched genes regulated by PPARδ, which requires further characterization. Interestingly, we found a unique EC1 cluster only expressed in $Ppard^{EC\text{-}KO}$, which express some markers of EC and FB, but are distinct from both cell types. *CD63* and *Col3a1* are the most highly expressed genes in EC1. *CD63*, one gene highly expressed in EC1, is involved in P-selectin dependent leukocyte recruitment [50], as well as other cellular processes such as integrin and VEGFR2 signaling in angiogenesis [51]. *Col3a1* is expressed in ECs and is implicated in EndoMT [52]. Moreover, several important genes which are reported to facilitate mesenchymal phenotype were upregulated in EC1 cluster, including *Junb*, *Mest*, and *Eif5a*. Interestingly, EC1 also had more similarities in gene expression with capECs, but with low expression of capEC markers *Cd300lg* and *Timp4* compared with capECs. We speculate that EC1 might be derived from capEC, which undergoes EndoMT possibly driven by hypoxia, oxidative stress, and inflammation [53], and become pro-inflammatory and pro-fibrotic due to the loss of PPARδ. However, not much is known whether PPARδ is involved in EndoMT. Nevertheless, our current result showed that PPARδ is essential to maintain endothelial homeostasis especially under injury and stress.

For treatment of patients with CLI, surgical operations are widely employed to reopen narrowed vessels or to construct revascularization. Therapeutic angiogenesis which aims to promote the development of new arteries and improve the perfusion of ischemic tissue, is considered as an idea alternative option for revascularization [54,55]. However, the efficacy of therapeutic angiogenesis is still not entirely clear. Based on the preclinical evidence showing the effect of several pro-angiogenic factors including, vascular endothelial growth factor (VEGF), fibroblast growth factor (FGF), and hepatocyte growth factors (HGF), a few clinical trials had been conducted to deliver angiogenic factors. For instance, initial trials showed the effectiveness of viral vector mediated delivery of VEGF165 by intra-arterial [56] or intramuscular [57,58] administration to overexpress VEGFA in ischemic muscle to increase vascularity, improving lower extremity endothelial function and flow reserve as well as VEGF121 [59]. However, other trials also showed lack of effect for VEGFA on especially the vascular functional outcomes and the endpoints such as walking performance and amputation rates [60,61].

FGF is another target considered for clinical trials. Although Phase I clinical study [62], and Phase II trials both showed better outcomes such as improvement of perfusion and lower risk of amputations after the treatment of NV1FGF [63], a larger Phase III trial of 525 patients did not show satisfactory results such as shortening the time to amputation or death [64]. The effect of another growth factor, HGF, which shows pro-angiogenic effect without causing vascular inflammation or affecting vascular permeability in preclinical study, was also tested in clinical trials [65]. VM202, a plasmid DNA expressing two isoforms of HGF was used in Phase I trial which was well tolerated, with a significant increase in median ABI and toe brachial pressure index (TBI) in the HGF-treated group at 12 months of follow-up [66]. In Phase II (clinicaltrials.gov nct01064440), ulcer healing and tissue oxygenation were improved in VM202-treated patients [67]. Although studies on the above gene therapeutic targets has entered in clinical stage, the evaluation of safety, efficacy and clinical primary endpoints (such as patient quality of life, amputation rate and other indicators) still need further evaluation. In addition to these growth factors, not much has been done to identify a feasible target which goes beyond angiogenesis to enhance the functionality of the repaired vasculature.

More recently, AAV has emerged as a promising alternative for achieving stable and safe transgene expression following in vivo delivery, and has been used in clinical trials. It would be an ideal vector for direct skeletal muscle gene transfer, which provides sustained gene expression, with minimally invasive procedures. In addition, without inducing significant vector-related inflammatory responses in the host. Here we showed two major advantages of local delivery of EC targeted gene delivery by rAAV directly: First, this method provides more efficient access of vector to ischemic tissue which avoids rAAV loss in circulation from blood flow to ischemic skeletal muscle; Second, targeted gene in ECs can be achieved to avoid potential non-specific effects in other cell types. In our study, we injected AAV locally into skeletal muscles and restricted the expression of PPARδ to ECs by constructing an EC-specific promoter ICAM2, in the attempt to reduce systemic side effects. Nevertheless, the potential side effects of AAV still need to be considered. The AAV vector DNA being integrated into genome of the infected cells rarely occurs but might causes genotoxic effects once happened.[68] Unexpected systemic leakage of AAV particles may also cause transduction of the target gene in untargeted cells or tissues, leading to mutations, resulting in the production of non-functional protein or abnormal proliferation [69–71]. In addition, different AAV capsids can induce cellular and humoral immune responses that generate anti-AAV antibodies to neutralize the vector, which prevent successful transduction of the target gene in the patients [68]. During the production of AAV vector, contamination by helper viruses, such as adenovirus, can lead to a strong immune response in the patient, especially if adenovirus is the helper virus [72].

Although animal studies showed that PPARδ agonists boost fatty acid utilization, and enhance physical endurance, and had been suggested as promising candidates for treating obesity and metabolic syndrome, they failed to reach the end point of clinical trials because of several side effects which cannot be ignored. GW501516, a well-known agonist, showed beneficial effects on obesity, insulin resistance, and reduction of plasma glucose in rodent models of type 2 diabetes. However, GW501516 was abandoned as a clinical drug due to increased risk of cancer in several preclinical animal studies [73,74], as well as GW0742 which showed similar adverse effects [74]. Nevertheless, investigating of differential mechanism of PPARδ action in different tissues and exploring suitable methods to regulate PPARδ based on specific disease models could still have clinical implications. In our study, different from using systemic delivery of pharmacological ligands, EC targeted delivery of AAV1-*Ppard* by direct local injection into the injured muscles resulted in notable improvement of disease outcome in mouse HLI model, without noticeable adverse reactions, suggesting its safety and efficacy.

While previous studies have already reported that PPARδ is involved in endothelial functions, most of which are based on the existing of PPARδ agonists, such as GW501516, GW0742, and L-165041. However, in current study, we unexpectedly find that the expression of PPARδ in ECs is significantly reduced at early stage of hindlimb ischemia (at days 3, Fig. 4a, b), which argues against the benefits obtained from those agonists if applied at this stage. In addition, our recent study also suggested a possibly ligand-independent effect of PPARδ in restoring endothelial homeostasis in the HLI model, via interaction with HIF1α [28], which also supports our current approach to first re-express PPARδ in ECs at early stage of HLI injury. Regarding the importance of both ligand-dependent and independent roles of PPARδ, it would be interesting to explore the synergistic effects of combining AAV-*Ppard* with agonists in those disease models in the future study.

In summary, our results demonstrate the critical protective roles of PPARδ in endothelial homeostasis in the context of obesity and insulin resistance. Gene therapy delivery of endothelial PPARδ by AAV1 could achieved favourable effects in ischemic muscles including: improving limb perfusion, increasing capillary density, decreasing muscle necrosis, and inhibiting inflammatory response. Our study emphasizes the potential therapeutic values of PPARδ on treating patients suffering PAD and CLI.

CRediT authorship contribution statement

Yalan Wu: Conceptualization, Data curation, Formal analysis, Investigation, Methodology, Visualization, Writing – original draft, Writing – review & editing. **Xiao Lin:** Formal analysis, Investigation, Methodology, Visualization, Writing – review & editing. **Huiling Hong:** Investigation. **Yee Lok Fung:** Investigation. **Xiaoyun Cao:** Investigation. **Joyce Ka Yu Tse:** Investigation. **Tsz Ho Li:** Investigation. **Ting Fung Chan:** Methodology, Resources, Writing – review &d editing. **Xiao Yu Tian:** Conceptualization, Data curation, Formal analysis, Funding acquisition, Methodology, Resources, Supervision, Visualization, Writing – original draft, Writing – review & editing.

Conflict of interest statment

The authors declare that they have no competing interests.

Data Availability

The raw datasets for this study have been deposited on NCBI with the accession ID: PRJNA691127. The datasets used and/or analyzed during the current study are available from the corresponding author upon reasonable request.

Acknowledgements

This study is supported by National Natural Science Foundation of China grants 81922078 and 32071145; Hong Kong Research Grant Council grants 14109519 and 14105321; Hong Kong Food and Health Bureau grant 08191156. Funding sources are used for experimental reagents and research staff salary; and are not involved in the writing of the manuscript, or the decision to submit it for publication. The authors have not been paid to write this article by a pharmaceutical company or other agency. The authors were not precluded from accessing data in the study and all the authors accept responsibility to submit for publication.

Appendix A. Supporting information

Supplementary data associated with this article can be found in the online version at doi:10.1016/j.biopha.2022.113172.

References

[1] M.E. Cooper, C.I. Johnston, Optimizing treatment of hypertension in patients with diabetes, JAMA 283 (24) (2000) 3177–3179.
[2] Z. Ali, et al., Peripheral artery disease in type II diabetes, J. Coll. Physicians Surg. Pak. 22 (11) (2012) 686–689.
[3] P. Song, et al., Global, regional, and national prevalence and risk factors for peripheral artery disease in 2015: an updated systematic review and analysis, Lancet Glob. Health 7 (8) (2019) e1020–e1030.
[4] A.W. Aday, K. Matsushita, Epidemiology of peripheral artery disease and polyvascular disease, Circ. Res 128 (12) (2021) 1818–1832.
[5] M. Vazquez-Carrera, Unraveling the effects of PPARbeta/delta on insulin resistance and cardiovascular disease, Trends Endocrinol. Metab. 27 (5) (2016) 319–334.
[6] F. Lovren, H. Teoh, S. Verma, Obesity and atherosclerosis: mechanistic insights, Can. J. Cardiol. 31 (2) (2015) 177–183.
[7] C.W. Hicks, et al., Associations of obesity with incident hospitalization related to peripheral artery disease and critical limb ischemia in the ARIC study, J. Am. Heart Assoc. 7 (16) (2018), e008644.
[8] H. Albadawi, et al., Hind limb ischemia-reperfusion injury in diet-induced obese mice, J. Surg. Res 190 (2) (2014) 683–691.
[9] L. Naldini, Gene therapy returns to centre stage, Nature 526 (7573) (2015) 351–360.
[10] S. Yla-Herttuala, A.H. Baker, Cardiovascular gene therapy: past, present, and future, Mol. Ther. 25 (5) (2017) 1095–1106.
[11] C. Zincarelli, et al., Analysis of AAV serotypes 1-9 mediated gene expression and tropism in mice after systemic injection, Mol. Ther. 16 (6) (2008) 1073–1080.
[12] Z. Wu, A. Asokan, R.J. Samulski, Adeno-associated virus serotypes: vector toolkit for human gene therapy, Mol. Ther. 14 (3) (2006) 316–327.
[13] M.L. Brantly, et al., Sustained transgene expression despite T lymphocyte responses in a clinical trial of rAAV1-AAT gene therapy, Proc. Natl. Acad. Sci. U.S.A. 106 (38) (2009) 16363–16368.
[14] F. Mingozzi, et al., AAV-1-mediated gene transfer to skeletal muscle in humans results in dose-dependent activation of capsid-specific T cells, Blood 114 (10) (2009) 2077–2086.
[15] J.R. Mendell, et al., Limb-girdle muscular dystrophy type 2D gene therapy restores alpha-sarcoglycan and associated proteins, Ann. Neurol. 66 (3) (2009) 290–297.
[16] A, P., European agency backs approval of a gene therapy. New York Times, New York, NY, in New York Times. 20 July 2012: New York, NY.
[17] L. Wang, et al., The pleiotropic effects of natural AAV infections on liver-directed gene transfer in macaques, Mol. Ther. 18 (1) (2010) 126–134.
[18] G.D. Hurlbut, et al., Preexisting immunity and low expression in primates highlight translational challenges for liver-directed AAV8-mediated gene therapy, Mol. Ther. 18 (11) (2010) 1983–1994.
[19] C. Li, et al., Neutralizing antibodies against adeno-associated virus examined prospectively in pediatric patients with hemophilia, Gene Ther. 19 (3) (2012) 288–294.
[20] T.E. Ryan, et al., PFKFB3-mediated glycolysis rescues myopathic outcomes in the ischemic limb, JCI Insight 5 (18) (2020).
[21] S.Y. Yoo, et al., Chimeric adeno-associated virus-mediated cardiovascular reprogramming for ischemic heart disease, ACS Omega 3 (5) (2018) 5918–5925.
[22] B. Grygiel-Gorniak, Peroxisome proliferator-activated receptors and their ligands: nutritional and clinical implications–a review, Nutr. J. 13 (2014) 17.
[23] E. Ehrenborg, J. Skogsberg, Peroxisome proliferator-activated receptor delta and cardiovascular disease, Atherosclerosis 231 (1) (2013) 95–106.
[24] Y. Fan, et al., Suppression of pro-inflammatory adhesion molecules by PPAR-delta in human vascular endothelial cells, Arterioscler. Thromb. Vasc. Biol. 28 (2) (2008) 315–321.
[25] J.M. Peters, Y.M. Shah, F.J. Gonzalez, The role of peroxisome proliferator-activated receptors in carcinogenesis and chemoprevention, Nat. Rev. Cancer 12 (3) (2012) 181–195.
[26] H. Yuan, et al., PPARdelta induces estrogen receptor-positive mammary neoplasia through an inflammatory and metabolic phenotype linked to mTOR activation, Cancer Res. 73 (14) (2013) 4349–4361.
[27] T. Adhikary, et al., Inverse PPARbeta/delta agonists suppress oncogenic signaling to the ANGPTL4 gene and inhibit cancer cell invasion, Oncogene 32 (44) (2013) 5241–5252.
[28] Y. Wu, et al., Endothelial PPARdelta facilitates the post-ischemic vascular repair through interaction with HIF1alpha, Theranostics 12 (4) (2022) 1855–1869.
[29] X. Sun, et al., MicroRNA-181b improves glucose homeostasis and insulin sensitivity by regulating endothelial function in white adipose tissue, Circ. Res. 118 (5) (2016) 810–821.
[30] H. Li, et al., Fibroblast growth factor 21 increases insulin sensitivity through specific expansion of subcutaneous fat, Nat. Commun. 9 (1) (2018) 272.
[31] T. Couffinhal, et al., Mouse model of angiogenesis, Am. J. Pathol. 152 (6) (1998) 1667–1679.
[32] T. Murohara, et al., Nitric oxide synthase modulates angiogenesis in response to tissue ischemia, J. Clin. Investig. 101 (11) (1998) 2567–2578.
[33] T. Stuart, et al., Comprehensive integration of single-cell data, Cell 177 (7) (2019) 1888–1902.e21.
[34] I. Tirosh, et al., Dissecting the multicellular ecosystem of metastatic melanoma by single-cell RNA-seq, Science 352 (6282) (2016) 189–196.
[35] V.K. Mootha, et al., PGC-1alpha-responsive genes involved in oxidative phosphorylation are coordinately downregulated in human diabetes, Nat. Genet. 34 (3) (2003) 267–273.
[36] A. Liberzon, et al., The Molecular Signatures Database (MSigDB) hallmark gene set collection, Cell Syst. 1 (6) (2015) 417–425.
[37] X. Huang, et al., Genome editing abrogates angiogenesis in vivo, Nat. Commun. 8 (1) (2017) 112.
[38] N. Wang, PPAR-delta in Vascular Pathophysiology, PPAR Res. 2008 (2008), 164163.
[39] S. Kutschera, et al., Differential endothelial transcriptomics identifies semaphorin 3G as a vascular class 3 semaphorin, Arterioscler. Thromb. Vasc. Biol. 31 (1) (2011) 151–159.
[40] F. Orsenigo, et al., Mapping endothelial-cell diversity in cerebral cavernous malformations at single-cell resolution, eLife 9 (2020), e61413.
[41] T. Su, et al., Single-cell analysis of early progenitor cells that build coronary arteries, Nature 559 (7714) (2018) 356–362.
[42] L.R. You, et al., Suppression of Notch signalling by the COUP-TFII transcription factor regulates vein identity, Nature 435 (7038) (2005) 98–104.
[43] J. Pan, et al., Patterns of expression of factor VIII and von Willebrand factor by endothelial cell subsets in vivo, Blood 128 (1) (2016) 104–109.
[44] M. Lee, et al., Transcriptional programs of lymphoid tissue capillary and high endothelium reveal control mechanisms for lymphocyte homing, Nat. Immunol. 15 (10) (2014) 982–995.
[45] A.C.A. Cleuren, et al., The in vivo endothelial cell translatome is highly heterogeneous across vascular beds, Proc. Natl. Acad. Sci. U.S.A. 116 (47) (2019) 23618.
[46] A.M. Gruntman, et al., Gene transfer in skeletal and cardiac muscle using recombinant adeno-associated virus, Curr. Protoc. Microbiol. (2013). Chapter 14: p. Unit 14D 3.
[47] O. Tornavaca, et al., ZO-1 controls endothelial adherens junctions, cell-cell tension, angiogenesis, and barrier formation, J. Cell Biol. 208 (6) (2015) 821–838.
[48] G.E. Rice, M.P. Bevilacqua, An inducible endothelial cell surface glycoprotein mediates melanoma adhesion, Science 246 (4935) (1989) 1303–1306.
[49] S. van Wetering, et al., VCAM-1-mediated Rac signaling controls endothelial cell-cell contacts and leukocyte transmigration, Am. J. Physiol. Cell Physiol. 285 (2) (2003) C343–C352.

[50] E.L. Doyle, et al., CD63 is an essential cofactor to leukocyte recruitment by endothelial P-selectin, Blood 118 (15) (2011) 4265–4273.
[51] S. Tugues, et al., Tetraspanin CD63 promotes vascular endothelial growth factor receptor 2-β1 integrin complex formation, thereby regulating activation and downstream signaling in endothelial cells in vitro and in vivo, J. Biol. Chem. 288 (26) (2013) 19060–19071.
[52] A.O. Samokhin, et al., NEDD9 targets COL3A1 to promote endothelial fibrosis and pulmonary arterial hypertension, Sci. Transl. Me.d 10 (445) (2018).
[53] X. Sun, et al., Endothelium-mediated contributions to fibrosis, Semin. Cell Dev. Biol. 101 (2020) 78–86.
[54] C. Inampudi, et al., Angiogenesis in peripheral arterial disease, Curr. Opin. Pharm. 39 (2018) 60–67.
[55] M. Nakatani, et al., Mechanisms of restenosis after coronary intervention: difference between plain old balloon angioplasty and stenting, Cardiovasc Pathol. 12 (1) (2003) 40–48.
[56] K. Makinen, et al., Increased vascularity detected by digital subtraction angiography after VEGF gene transfer to human lower limb artery: a randomized, placebo-controlled, double-blinded phase II study, Mol. Ther. 6 (1) (2002) 127–133.
[57] A. Arveschoug, K.S. Christensen, Constitutive expression of phVEGF165 after intramuscular gene transfer promotes collateral vessel development in patients with critical limb ischemia, Circulation 99 (22) (1999) 2967–2968.
[58] J.M. Isner, et al., Treatment of thromboangiitis obliterans (Buerger's disease) by intramuscular gene transfer of vascular endothelial growth factor: preliminary clinical results, J. Vasc. Surg. 28 (6) (1998) 964–973.
[59] S. Rajagopalan, et al., Adenovirus-mediated gene transfer of VEGF(121) improves lower-extremity endothelial function and flow reserve, Circulation 104 (7) (2001) 753–755.
[60] Y.H. Kusumanto, et al., Treatment with intramuscular vascular endothelial growth factor gene compared with placebo for patients with diabetes mellitus and critical limb ischemia: a double-blind randomized trial, Hum. Gene Ther. 17 (6) (2006) 683–691.
[61] S. Rajagopalan, et al., *Regional angiogenesis with vascular endothelial growth factor in peripheral arterial disease: a phase II randomized, double-blind, controlled study of adenoviral delivery of vascular endothelial growth factor 121 in patients with disabling intermittent claudica*tion, Circualtion 108 (16) (2003) 1933–1938.
[62] A.J. Comerota, et al., Naked plasmid DNA encoding fibroblast growth factor type 1 for the treatment of end-stage unreconstructible lower extremity ischemia: preliminary results of a phase I trial, J. Vasc. Surg. 35 (5) (2002) 930–936.
[63] S. Nikol, et al., Therapeutic angiogenesis with intramuscular NV1FGF improves amputation-free survival in patients with critical limb ischemia, Mol. Ther. 16 (5) (2008) 972–978.
[64] J. Belch, et al., Effect of fibroblast growth factor NV1FGF on amputation and death: a randomised placebo-controlled trial of gene therapy in critical limb ischaemia, Lancet 377 (9781) (2011) 1929–1937.
[65] T. Kaga, et al., Hepatocyte growth factor stimulated angiogenesis without inflammation: differential actions between hepatocyte growth factor, vascular endothelial growth factor and basic fibroblast growth factor, Vasc. Pharm. 57 (1) (2012) 3–9.
[66] T.D. Henry, et al., Safety of a non-viral plasmid-encoding dual isoforms of hepatocyte growth factor in critical limb ischemia patients: a phase I study, Gene Ther. 18 (8) (2011) 788–794.
[67] M.R. Kibbe, et al., Safety and efficacy of plasmid DNA expressing two isoforms of hepatocyte growth factor in patients with critical limb ischemia, Gene Ther. 23 (3) (2016) 306–312.
[68] P. Colella, G. Ronzitti, F. Mingozzi, Emerging issues in AAV-mediated in vivo gene therapy, Mol. Ther. Methods Clin. Dev. 8 (2018) 87–104.
[69] M.F. Naso, et al., Adeno-associated virus (AAV) as a vector for gene therapy, BioDrugs 31 (4) (2017) 317–334.
[70] G.M. Thomsen, et al., Systemic injection of AAV9-GDNF provides modest functional improvements in the SOD1(G93A) ALS rat but has adverse side effects, Gene Ther. 24 (4) (2017) 245–252.
[71] S.S. Gill, et al., Direct brain infusion of glial cell line-derived neurotrophic factor in Parkinson disease, Nat. Med. 9 (5) (2003) 589–595.
[72] D. Wang, P.W.L. Tai, G. Gao, Adeno-associated virus vector as a platform for gene therapy delivery, Nat. Rev. Drug Discov. 18 (5) (2019) 358–378.
[73] R.A. Gupta, et al., Activation of nuclear hormone receptor peroxisome proliferator-activated receptor-delta accelerates intestinal adenoma growth, Nat. Med. 10 (3) (2004) 245–247.
[74] X. Wang, et al., PPAR-delta promotes survival of breast cancer cells in harsh metabolic conditions, Oncogenesis 5 (6) (2016), e232.